machines

IMPACT FACTOR 2.1

CITESCORE 4.7

Article

Wear and Plasticity in Railway Turnout Crossings: A Fast Semi-Physical Model to Replace FE Simulations

Hamed Davoodi Jooneghani, Kamil Sazgetdinov, Alexander Meierhofer, Stephan Scheriau, Uwe Ossberger, Gabor Müller and Klaus Six

Special Issue

Wheel–Rail Contact: Mechanics, Wear and Analysis

Edited by

Prof. Dr. Andrea Bracciali and Dr. Gianluca Megna

MDPI

https://doi.org/10.3390/machines13020105

machines

MDPI

Article

Wear and Plasticity in Railway Turnout Crossings: A Fast Semi-Physical Model to Replace FE Simulations †

Hamed Davoodi Jooneghani [1,2,*], Kamil Sazgetdinov [1], Alexander Meierhofer [1], Stephan Scheriau [3], Uwe Ossberger [3], Gabor Müller [1] and Klaus Six [1]

[1] Virtual Vehicle Research GmbH, Inffeldgasse 21A, 8010 Graz, Austria
[2] Institute of Materials Science, Joining and Forming, Graz University of Technology, Kopernikusgasse 24/I, 8010 Graz, Austria
[3] Voestalpine Rail Technology GmbH, Kerpelystraße 199, 8700 Leoben, Austria
* Correspondence: davoodijooneghani@student.tugraz.at or hamed.davoodi@v2c2.at
† This paper was presented at the 12th International Conference on Contact Mechanics and Wear of Rail/Wheel Systems, Melbourne, Australia, 4−7 September 2022. It has been extended for publication in this journal.

Abstract: Severe changes in the profiles of the crossing nose are caused by large dynamic contact forces. To predict these forces as well as the profile evolution, the Whole System Model (WSM) was developed. However, it uses computationally expensive FE simulations. As a replacement, the semi-physical plasticity and wear model (SPPW) has been developed, thus majorly enhancing the overall performance of the WSM. The SPPW considers the influence of wear, plasticity, and wheel-profile-related effects. Its results have shown an overall good correlation with FE results, laboratory data for different materials, and field data from a real crossing. Due to the semi-physical nature of the model, the required computational time for the predictions was significantly reduced compared to FE simulations: minutes instead of weeks. The SPPW will be useful for time-efficient rail damage prediction, like wear and plastic deformation, and, as part of the WSM, contribute to a fast holistic track damage prognosis.

Keywords: wheel-rail contact mechanics; material plasticity modeling; railway turnout; switches and crossings; MBD simulation; FE-method; semi-physical plasticity modeling; Hertzian contact

Academic Editors: Andrea Bracciali and Gianluca Megna

Received: 2 December 2024
Revised: 22 January 2025
Accepted: 24 January 2025
Published: 28 January 2025

Citation: Davoodi Jooneghani, H.; Sazgetdinov, K.; Meierhofer, A.; Scheriau, S.; Ossberger, U.; Müller, G.; Six, K. Wear and Plasticity in Railway Turnout Crossings: A Fast Semi-Physical Model to Replace FE Simulations. *Machines* **2025**, *13*, 105. https://doi.org/10.3390/machines13020105

1. Introduction

Large dynamic contact forces in railway switches, turnouts, and crossings result from discontinuities in wheel-rail contact geometry. The accumulation of such dynamics can lead to degradation and damage of rail surfaces, such as profile changes due to wear, massive plastic deformation, rolling contact fatigue, as well as track irregularities [1]. In [1], the so-called whole system model (WSM) was presented, which predicts the development of rail wear, plasticity, and vertical track geometry in an integrated, holistic way, as shown in Figure 1.

The multibody dynamics (MBD) simulations in WSM capture vehicle-turnout interactions, including the wheel-rail contact forces and the effects of varying wheel profiles. These forces are inputs for the Vehicle-Track Interaction (VTI) model, which predicts track settlement over time [2] (see the lower left part of Figure 1).

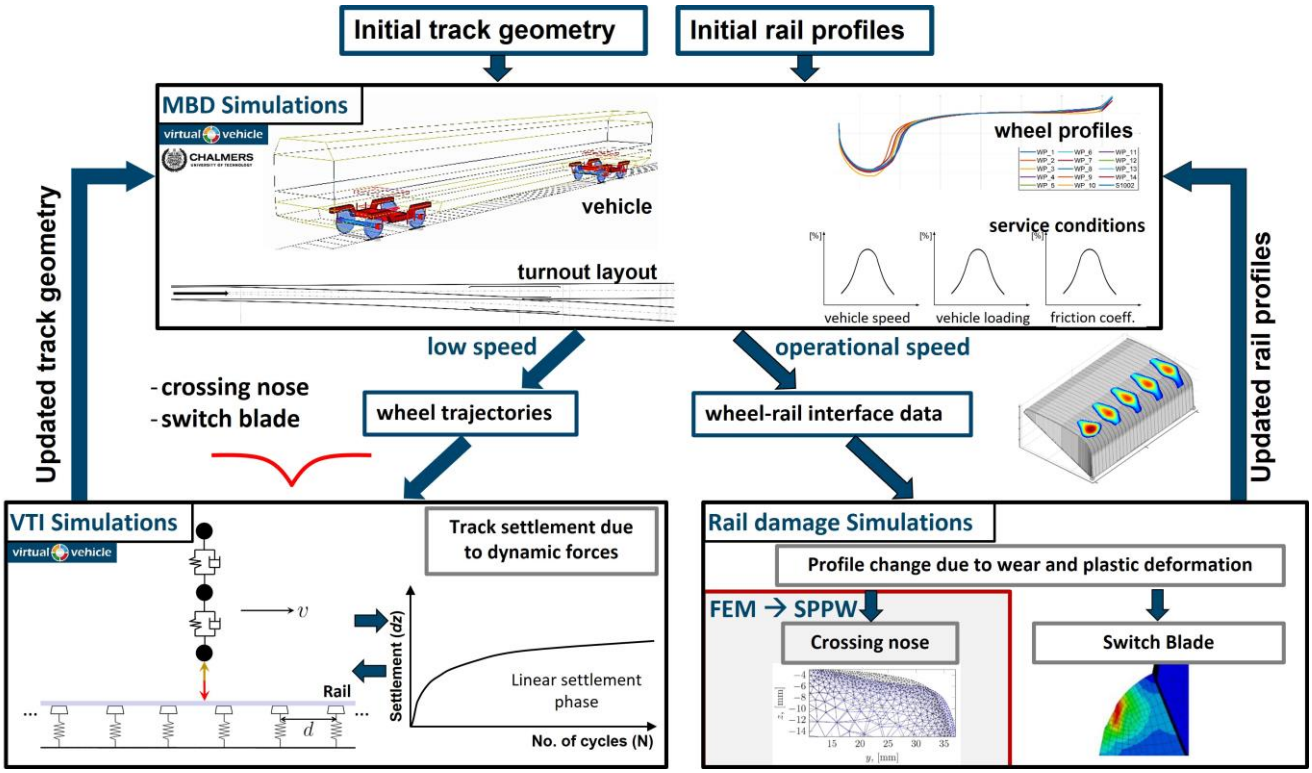

Figure 1. Whole system model (WSM) for the track damage predictions in railway turnouts [1]. The calculation times are taken from the demonstration example in [1] and indicate the computational effort required for the different steps.

As described in the lower right part of Figure 1, rail profile changes due to plastic deformation and wear are calculated using FE simulation based on these dynamic forces. The Ohno–Wang model [3], which combines isotropic and kinematic hardening, is used to account for cyclic plastic deformation. The wear model used is based on Archard [4].

The chosen approach is known from the literature, where many researchers also use hybrid iterative combinations of MBD and Finite Element (FE) simulations [5–7]. By iteratively updating the track geometry and rail profiles based on traffic load, the WSM provides a holistic approach to assessing turnout damage [1].

While the results were quite promising [1], the FE simulations were found to cause the highest computational effort, extending the run of the full loop to several weeks. Therefore, this work aims to demonstrate a novel time-efficient semi-physical plasticity and wear model (SPPW) to replace the FE simulations in the WSM. The first idea of SPPW was presented in 2022 [8] but further developed by including new investigations based on laboratory tests and field data. It can be used more effectively for long-term track condition assessments by, for example, turnout suppliers to optimize both design and material selection for turnout crossings. This will help to reduce the risk of unplanned maintenance actions like the renewal of turnout components caused by wear and plastic deformation, thereby saving costs. Previously, there was no fast and reliable way to predict deformations in early design stages, but the SPPW method fills this gap.

2. Modeling

This study proposes the semi-physical plasticity and wear metamodel (SPPW) to predict the rail profile evolution in the crossing nose region, one of the most heavily loaded areas in railway turnouts. The main contributions to this crossing nose rail profile evolution are caused by plastic deformation and wear. Plastic deformation is more dominant during

the early stages of the nose's life cycle, directly following installation or maintenance actions. Several cross-disciplinary simulation methodologies have been analyzed, such as [9–11], aimed at modelling this phenomenon accurately and time-efficiently. Ultimately, a calibrated FE model was used in the WSM to simulate the railway turnout degradation, prioritizing accuracy before time efficiency [1]. The results should serve as a basis for further investigations of plasticity modeling and the development of a more time-efficient surrogate model. The study in [1] employs FE results to model the cyclic plastic deformation and wear of rail components, particularly in the critical areas of switches and crossings, which are susceptible to significant damage due to the dynamic loads from passing trains. The FE results (see Figure 2), specifically for the switchblade and crossing nose, highlight the changes in rail profiles made from R350HT rail material due to plastic deformation and wear for 38 cross-sections.

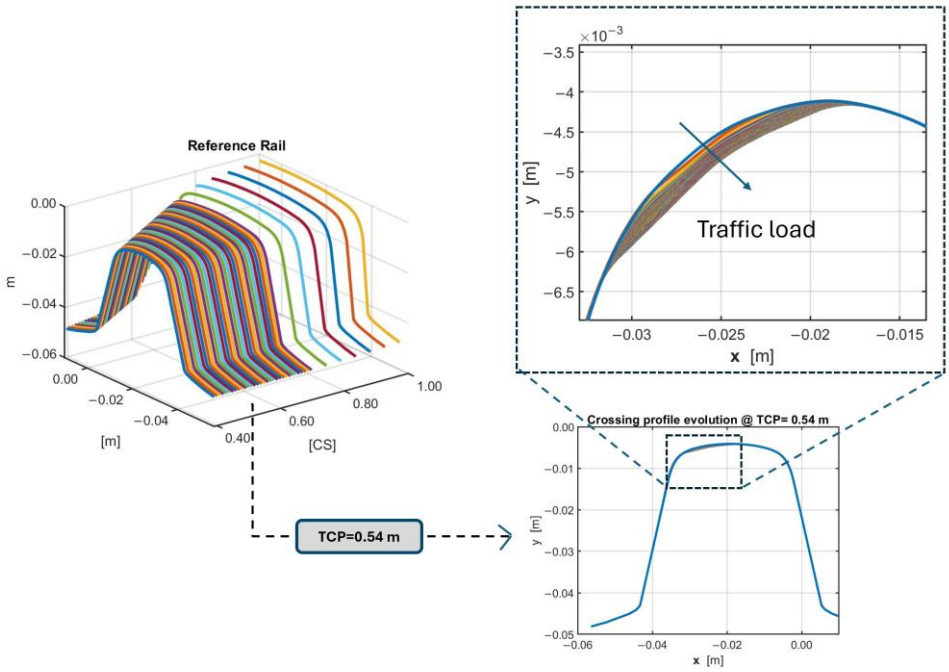

Figure 2. The schematic representation of the crossing rail profiles used in FE simulation and an example of the crossing nose profile evolution at 0.54 m from the theoretical crossing point (TCP).

Within the WSM framework, multibody dynamics (MBD) simulations in the Simpack environment are used (Figure 1). These simulations use a full-scale vehicle model parametrized based on the Manchester Benchmark Vehicle [12] and a commonly used Swedish turnout layout from the Switching and Crossing simulation Benchmark [13]. A set of measured wheel profiles, as shown as the envelope of wheel profiles in Figure 3b, has been used (representing different wear conditions during the operation of the train on the track) to replicate the realistic track operating conditions [14]. The parametrized MBD model generates wheel-rail contact interface data such as maximum Hertzian contact pressure, contact patch dimensions, and creepages to be used as input for rail damage FE simulation to predict the evolution of the crossing nose profiles, as can be seen in the lower right block in Figure 1.

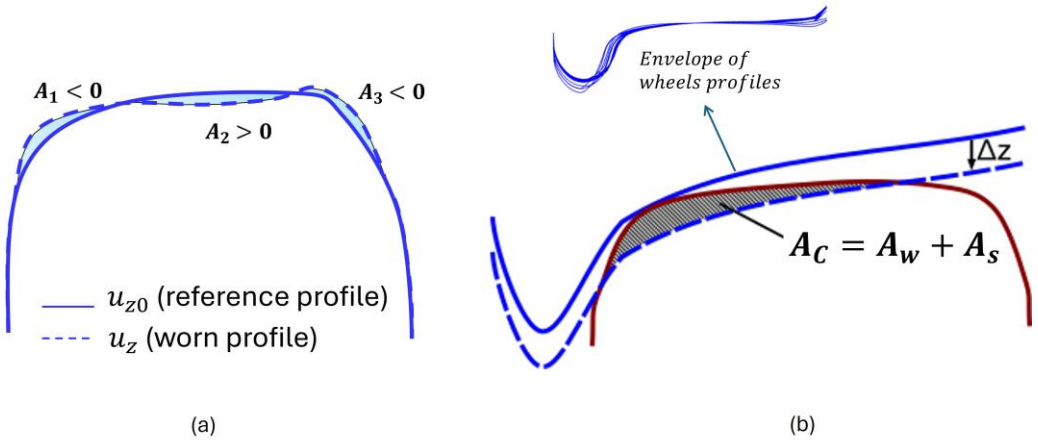

Figure 3. (**a**) Reference and worn profiles (**b**). Sketch of the shift along the *z*-axis of the envelope of all wheel profiles so that the change area (A_c) equals the wear area (A_W) plus the shape change area (A_s) with the assumption of the accumulative wheel profile envelope effect on the rail profile shape evolution.

The SPPW is based on the idea that the envelope of the traversing wheels acts like a grinder. Therefore, the wheel profile envelope can be shifted vertically (Δz) until the region of overlap between the wheel profile envelope and the rail is the same as the Change Area (A_C). This is shown in Figure 3b. While the wheel profile envelope is derived from the MBD simulation results, A_C is the sum of the wear area (A_w) and the shape change area (A_S) due to plastic deformation:

$$A_C = A_w + A_s, \tag{1}$$

So, knowing A_w and A_s, the Change Area is defined, and the shift in the profile envelope can be derived.

1. The wear area (A_w) for each rail profile cross-section (CS) can be calculated by:

$$A_w(L_g) = \int_{y_0}^{y_1} \left(u_{z0} - u_z(L_g)\right)\ \mathrm{d}y = \sum_i A_i, \tag{2}$$

where u_{z0} is a vertical coordinate of the reference (in our case—initial) profile cross-section and u_z is the actual vertical coordinate of the current cross-section at a given gross traffic load L_g. A_1, A_2 and A_3 are the distinct areas of profile changes as described in Figure 3a. It is important to clarify that the wear area refers to the material removed from the rail surface due to the wear process.

Since it is very hard to link the wear area itself to physical quantities, it was rather chosen to use the wear rate (g_w), which is the derivative of the wear area with respect to load L_g:

$$g_w(L_g) = \left.\frac{dA_w}{dL_g}\right|_{L_g} \approx \frac{A_w(L_g) - A_w(L_g - \Delta L_g)}{\Delta L_g}, \tag{3}$$

2. The shape change area (A_s) is calculated as an integral over the profile length, subtracting the wear area [15]:

$$A_s(L) = \frac{1}{2} * \left(\int_{y_0}^{y_1} |u_{z0} - u_z(L)|\ \mathrm{d}y - A_w(L)\right) = \frac{1}{2}\left(\sum_i |A_i| - A_W\right), \tag{4}$$

where u_{z0} is a vertical coordinate of the reference profile cross-section (see Figure 3a) and u_z is the actual vertical coordinate of the current cross-section at the given gross traffic load L_g.

The shape change area represents the profile change due to plastic deformation.

Similarly to the wear area, the shape change rate g_s is defined as the gradient of the shape change area over traffic load:

$$g_s(L_g) = \left.\frac{dA_s}{dL_g}\right|_{L_g} \approx \frac{A_s(L_g) - A_s(L_g - \Delta L_g)}{\Delta L_g}, \quad (5)$$

FE results, laboratory data, or field tests can be used to link the wear rate, and the shape change rate to physical quantities.

3. Testing

In addition to the FE Data from the literature in this work [1], two types of measurements were used. The first is a specially designed laboratory test at the full-scale linear test rig of voestalpine Rail Technologies GmbH in Leoben, Austria. The second one is data from a crossing in real operation.

3.1. Laboratory Tests

Special laboratory tests were performed for this work to avoid relying purely on FE simulation data. There, the behavior of different materials was investigated at the linear full-scale test rig of voestalpine [16,17]. Modified rails, which narrowed in a longitudinal direction, were used. The exact specifications are depicted in Figure 4. The rails were then cyclically loaded with a cylindrical wheel, and after each predefined number of cycles, the profiles on six different cross-sections were measured. In the voestalpine test rig (VTR) setup, the modified rails of various materials are in contact with a rolling cylindrical wheel of 500 mm. The wheel exerted a normal load on the rails, ranging from approximately 12 to 40 t. For each load step (~12, ~20, ~30, and ~40 t), a set number of load cycles was applied to reach a constant steady load condition through several cycles, and the corresponding traffic load was determined. Each material underwent a total of 40,000 load cycles. Due to the circular shape of the rail head with varying diameters and the increasing normal load throughout the experiments, the maximum contact stress varies, leading to a calculated traffic load between 0 and 1.4 MGT. The test rig (TR) system maintained zero spin slippage and no lateral or longitudinal slippage during the tests.

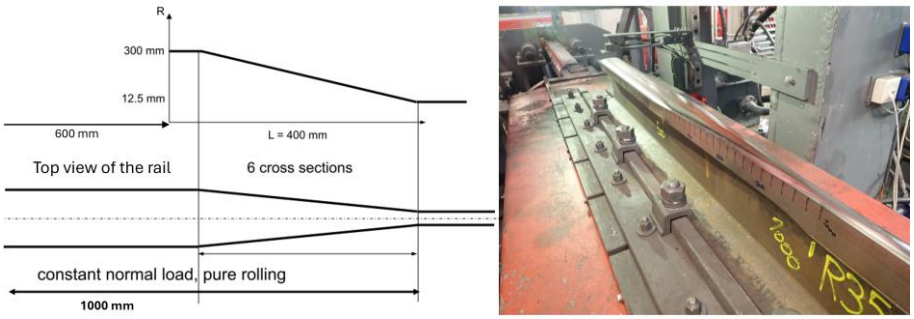

Figure 4. Specification of the modified rail used in the testing. (**a**). Top view of the modified rail. (**b**). The modified rail was used in the testing.

During the tests, the behavior of five different rail materials was investigated. These were the standard rail steels: R260, R350HT, R400HT, standard turnout cast manganese steel (Mn), and standard turnout explosive-depth-hardened cast manganese steel (Mn_EDH).

Figure 5 shows the results of profile evolution for all materials at the smallest cross-section (CS 1000 mm). It must be noted that the top of the profiles with the most cycles is not parallel with the y-axis. This might be due to the wheel disk being bent under the load.

Figure 5 shows that the plastic deformation is lower for R400HT and R350HT materials. Additionally, all materials exhibit more significant deformation during the initial phase, contributing to material hardening.

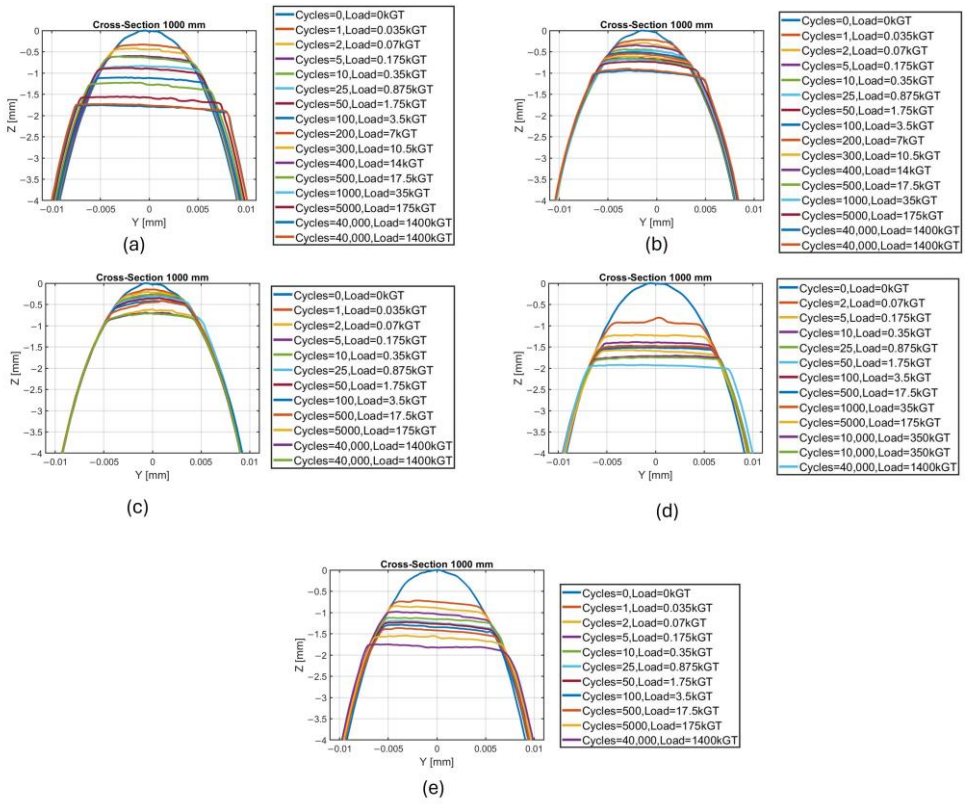

Figure 5. Results for cross-sections at 1000 mm distance (see Figure 4a) for (**a**). R260, (**b**). R350HT, (**c**). R400HT, (**d**). Mn, and (**e**). Mn_EDH.

3.2. Field Data

In addition to the tests in the test rig, field measurements offer important real-world data and enable a more complete understanding of the material's performance. The investigated crossing is in Niklasdorf and runs under real operational conditions in the ÖBB network. A prototype crossing nose consisting of Mn_EDH material is installed. It is estimated that the crossing rails experienced approximately 100 MGT traffic loads during the measurement period. Ten profile measurements (see Table 1) have been taken (M01, M02, . . . , M10) between 12 November 2012 and 22 August 2017 at Niklasdorf crossing 5 (ND5). An example of a certain cross-section measurement is shown in Figure 6. These data allow for the close investigation of wear and deformation at a Mn_EDH crossing nose under real operational conditions. The field tests were conducted under mixed all-weather conditions across multiple seasons, and the line accommodates passenger and freight traffic in both directions. During the tests, the train's operating speed was approximately 100 km/h.

Table 1. Profile measurement intervals at ND5.

	M01	M02	M03	M04	M05	M06	M07	M08	M09	M10
Date	12 November 2012	18 February 2013	27 May 2013	02 September 2013	31 March 2014	08 September 2014	26 March 2015	30 November 2015	25 July 2016	22 August 2017
Traffic load [MGT]	0	6	11	17	29	38	50	64	78	100

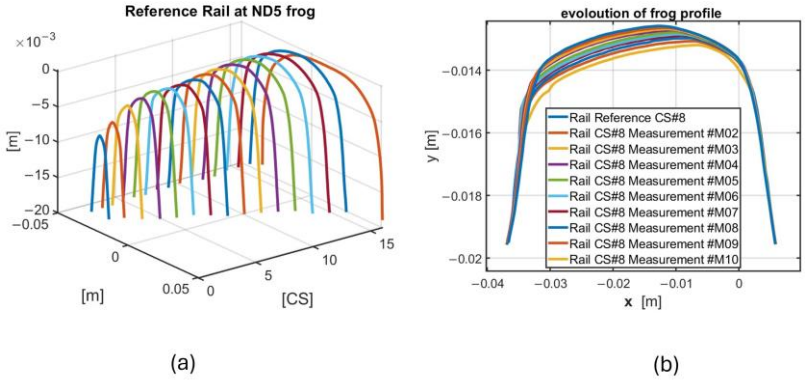

Figure 6. (**a**) 3D graph of the reference crossing nose (M01) showing rail profile at different cross-sections. (**b**). Profile evolution of cross-section #8 at the distance of 350 mm from TCP (theoretical crossing point).

4. Model Calibration

Test rig data (TR) for five materials and data from previous FE simulations for R350HT were available for calibration. These data was used to derive the dependencies of the wear rate (g_W) and the shape change rate (g_S) (see Equations (3) and (5)) and use it to calibrate the SPPW.

The calibration results for R350HT are shown in Figure 7. Here, FE and laboratory results were used. It can be seen that the wear rate (g_W) was linearly related to the wear number (T_γ) with two empirical parameters k and d:

$$g_W(T_\gamma) = kT_\gamma + d, \tag{6}$$

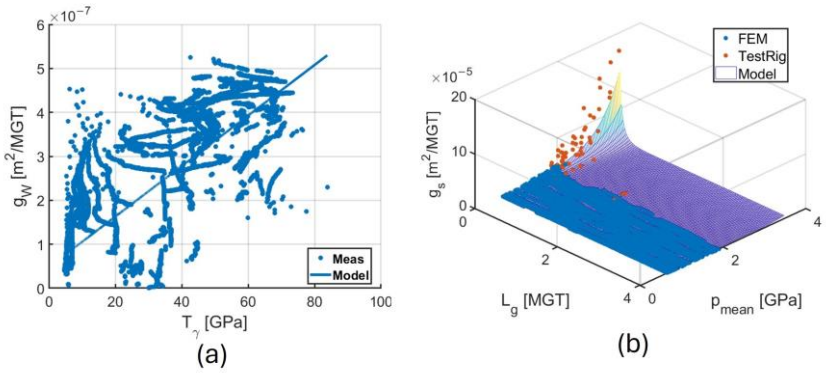

Figure 7. (**a**). Wear area rate, dots for FE-measurement, and line is the model (**b**). Shape change area rate for R350HT, red dots for measurement from the test rig, blue dots for FE-data, and the graph is the model with R^2 value of 0.72.

Similarly, the shape change rate (g_S) was related to L_g as well as the mean pressure in the contact (p_m). A multiterm exponential form (Equation (7)) was used to reproduce the results by finding the constants c_0, c_1, c_2, c_3, c_4, c_5, c_6 for the given material, e.g., R350HT.

$$g_s(p_m, L_g) = c_0 + c_1 exp^2\left(\frac{p_m - c_2}{c_3}\right) + \frac{c_4}{L_g + c_6} + \frac{c_5}{L_g + c_6} exp^2\left(\frac{p_m - c_2}{c_3}\right) + \frac{c_5}{(L_g + c_6)^2} exp^2\left(\frac{p_m - c_2}{c_3}\right), \quad (7)$$

The calibration results for R260, R400HT, Mn, and Mn-EDH are shown in Figure 8. The SPPW for VTR was calibrated specifically to reflect the shape changes observed in the experimental data for various materials tested at VTR. The formula mentioned in Equation (7) was applied for the shape change component, fitting the shape change area data primarily driven by plastic deformation under pure rolling conditions with a cylindrical wheel. In the VTR experiments, the changes in the plastic area were dominant, with most of the profile evolution resulting from plastic deformations rather than wear because of the pure rolling cylindrical wheel without an angle of attack. The dominance of plastic deformation in the profile evolution, as observed in the VTR experiments, indicated that incorporating a wear area model would not significantly enhance the accuracy of the predictions.

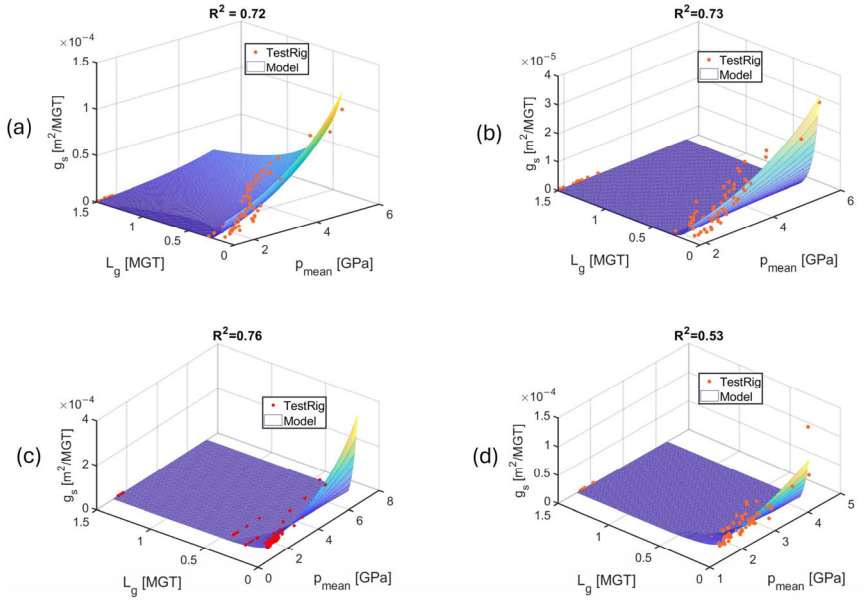

Figure 8. Calibrated shape change rate model for (**a**). R260 in VTR (**b**). R400HT in VTR (**c**). Mn in VTR (**d**). Mn-EDH in VTR.

5. Model Comparisons and Applications

The calibrated SPPW was used in three different applications and compared to either simulation results or test data to analyze its performance and the quality of its prediction. The first scenario is reproducing the FE results for R350HT from the literature. The second is the reproduction of the laboratory tests from the test rig for all five materials. This helps to understand the uncertainties and deviations introduced by the model simplifications and assumptions. The third scenario is predicting the field data previously presented in Section 3.2.

5.1. Reproduction of FE Data for R350HT

The SPPW, calibrated for R350HT, described in Figure 7 and Equations (6) and (7), was combined with MBD simulation using the Swedish turnout layout from the S&C simulation benchmark similar to the previous research [1]. As the results of the MBD simulation, the shape change area and wear area were estimated using SPPW and compared to the FE data. The results are shown in Figure 9 for 38 cross-sections. In this figure, the area changes

for wear and shape change are predicted nicely and are approximately equal to the area changes from FE results. The root mean square error (RMSE) between the shape change and wear area calculated from the FE-data and the SPPW for the R350HT crossing is shown in Figure 10 for cross-sections between 8 and 30. For these cross-sections, the RMSE value is approximately below 30% for all cross-sections, and the average RMSE for wear area and shape change area are, respectively, 12.51% and 8.55%, which is acceptable considering how much faster the SPPW is compared to the FE method for shape change and wear area estimation. RMSE is not calculated for other cross-sections, likely because in the MBD simulation process performed in [1], there is a lack of wheel-rail contact at these cross-section positions, leading to significantly underestimated area changes in these regions.

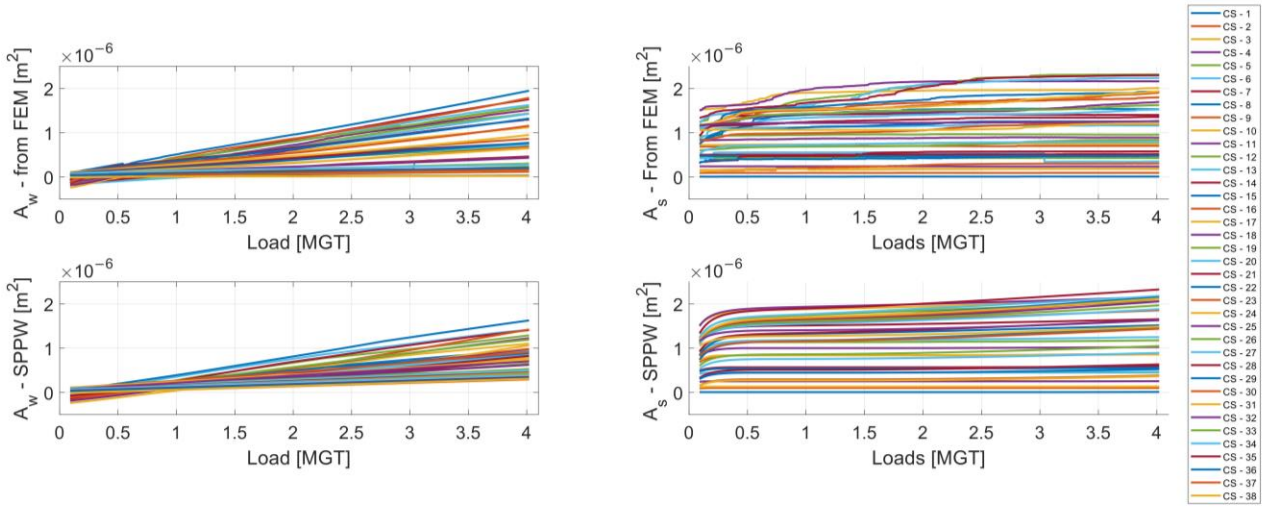

Figure 9. Comparison of the area changes calculated from the SPPW and FE results for R350HT crossing.

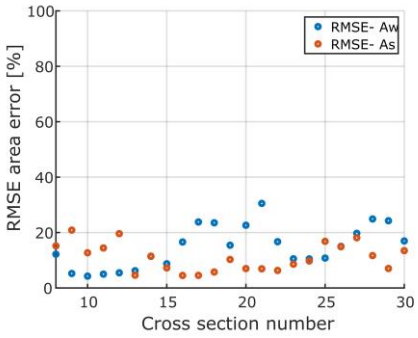

Figure 10. Root mean square error of shape change area (As) and wear area (Aw) for R350HT crossing numbers between 8 and 30. Crossing section number 8 is at the 0.46 m distance from the theoretical crossing point. Crossing section number 30 is at the 0.68 m distance from the theoretical crossing point.

Additionally, a selection of the predicted crossing nose profiles using the SPPW is displayed in Figure 11 after 3.5 MGT of traffic load. These profiles were predicted by considering the overall area changes, including the shape change and wear areas. The evolution of these profiles is influenced by the wheel profile envelope, as discussed in the materials and methods section. These profiles are sectioned at distances of 0.48 m, 0.54 m, and 0.58 m from the theoretical crossing point and compared to the corresponding profiles in FE results. The predicted profiles obtained from the SPPW method align well with the FEM results and accurately capture the overall shape in the FE simulations, confirming the effectiveness of the SPPW methodology.

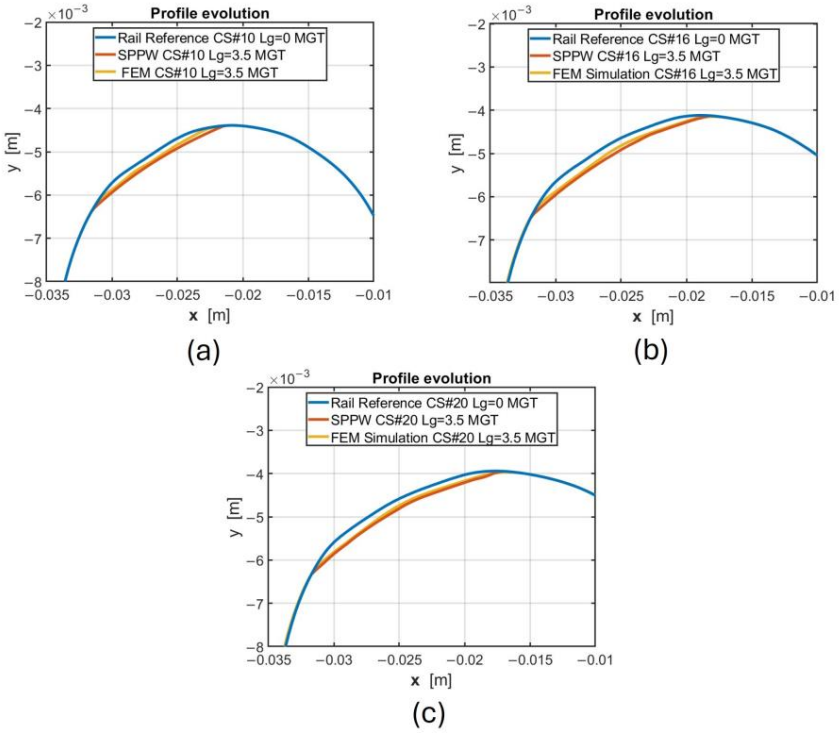

Figure 11. Profile evolution using the SPPW and comparison to crossing nose profiles calculated from FE data. (**a**) CS #10 at 0.48 m distance from TCP. (**b**) CS #16 at 0.54 m distance from TCP. (**c**) CS #20 at 0.58 m distance from TCP.

It must be noted that the decrease in computational effort was very significant. In contrast to the FE measurements, which took several weeks, the SPPW could predict the results on a standard laptop in seconds, minutes at worst. This reduced the time necessary to calculate the whole WSM loop to hours instead of weeks and introduced the MBD simulations as a new bottleneck of the WSM algorithm.

So, in summary, although there are deviations regarding the results, the significant decrease in calculation time indicates that the simplified SPPW prediction approach, which includes considerations for both wear and plastic deformation, is well suited for estimating the evolution of rail profiles under dynamic loading conditions.

5.2. Reproduction of the Fullscale Laboratory Tests for Different Materials

The calibrated SPPW was used to reproduce the laboratory test results at the voestalpine full-scale linear test rig to investigate the model's capabilities and analyze the uncertainties introduced by the model simplifications and assumptions. Since the wear was negligible (see Section 3.1), only the shape change area and, thus, the plastic behavior could be predicted. The results of profile evolution for R350HT are shown in Figure 12a,f. The simulated profiles closely match the experimental results, demonstrating the accuracy and reliability of the SPPW approach in capturing the key aspects of profile evolution. This alignment confirms that the SPPW can effectively simulate cross-profile evolution under varying operational conditions observed. The calibrated SPPW (see Figure 8) was also employed to simulate the profile evolution of other crossing rail materials based on experimental data from the voestalpine test rig (VTR), including R260, R400HT, Mn, and Mn_EDH. Figure 12 compares these predicted profiles with the corresponding profiles obtained from the test rig for different materials. This figure illustrates the model's performance across different materials, showcasing its adaptability and effectiveness in simulating profile evolution and shape changes for various crossing rail material types. Inaccuracies in the measurement process and the limited data points available for the

crossing nose profile material may have impacted the model's calibration. As a result, the SPPW-predicted profile shows some discrepancies, as seen in Figure 12j, which can be attributed to the measurement errors.

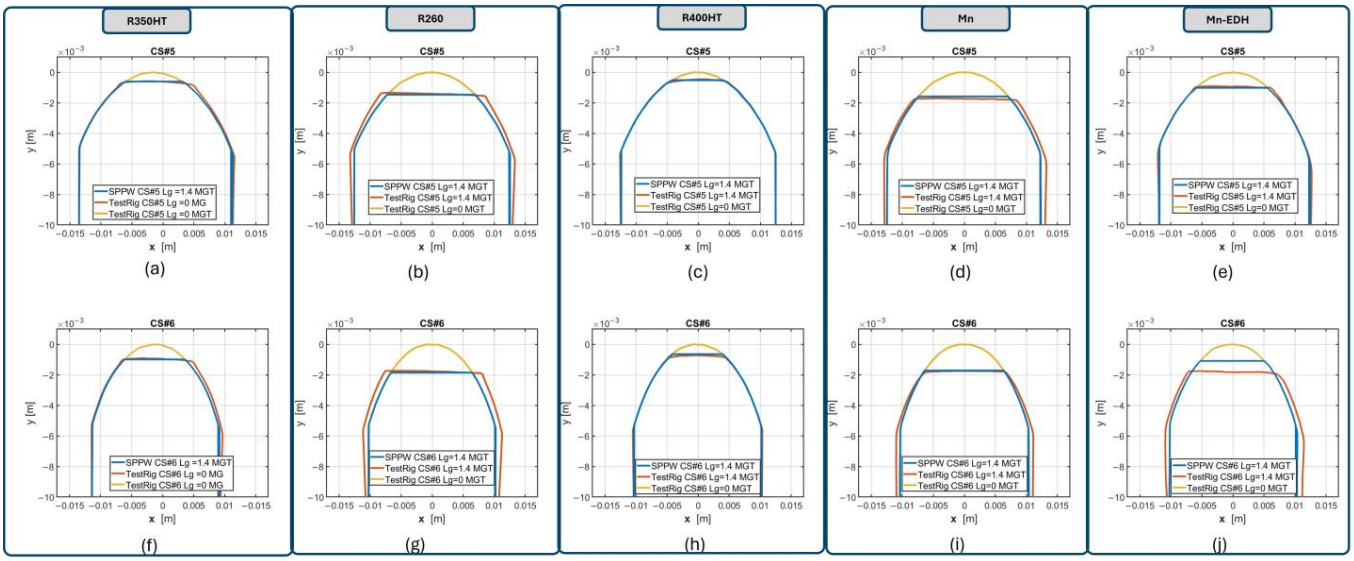

Figure 12. Comparison of SPPW and test rig data on a profile level. (**a**). Profile evolution for R350HT at cross-section 5 at 950 mm *distance. (**b**). Profile evolution for R260 at cross-section 5 at 950 mm *distance. (**c**). Profile evolution for R400HT at cross-section 5 at 950 mm *distance. (**d**). Profile evolution for Mn at cross-section 5 at 950 mm *distance. (**e**). Profile evolution for Mn-EDH at cross-section 5 at 950 mm *distance. (**f**). Profile evolution for R350HT at cross-section 6 at 1000 mm *distance. (**g**). Profile evolution for R260 at cross-section 6 at 1000 mm *distance. (**h**). Profile evolution for R400HT at cross-section 6 at 1000 mm *distance. (**i**). Profile evolution for Mn at cross-section 6 at 1000 mm *distance. (**j**). Profile evolution for Mn-EDH at cross-section 6 at 1000 mm *distance. *Distances are based on Figure 4a.

It must be noted that the SPPW results can only be valid within the actual contact. Changes outside of this area, like material flow and the plastic deformation at the sides of the rail head, cannot be predicted, as shown in Figure 12b,d,f,g,i,j.

The materials used in the VTR and modeled with the SPPW exhibit different behaviors, and the model effectively captures these variations. For instance, the shape change area is predicted to be higher for R260 than R400HT, which can be attributed to the lower hardness of R260.

5.3. SPPW Method Application and Feasibility Check for a Crossing at Niklasdof (ND5)

The SPPW feasibility check and application involved collecting ten measurement data points over different intervals to monitor profile evolution at crossing 5 in Niklasdorf, which utilizes Mn-EDH material. To assess the feasibility of the SPPW, an MBD simulation was developed using the same vehicle and conditions as described for the R350HT FE data. An in-house method [18] was employed to align the profiles, involving creating and aligning a 3D mesh and extracting aligned profiles for use in the MBD simulation. Aligning profiles is particularly important for measurement data because it requires proper alignment, unlike FE data, which is already inherently aligned. This is why the specific meshing methodology is used. An example of an aligned and rotated mesh based on reference rail profiles (M01) is shown in Figure 13. The SPPW used, in this case, consisted of a shape change model calibrated from the VTR shape change model for Mn-EDH material. For the wear rate model, the slope of the wear rate model (k in Equation (6)) was adjusted to be 70% steeper than that of R350HT. This modification is based on Archard's wear model, indicating that harder materials resist wear more effectively.

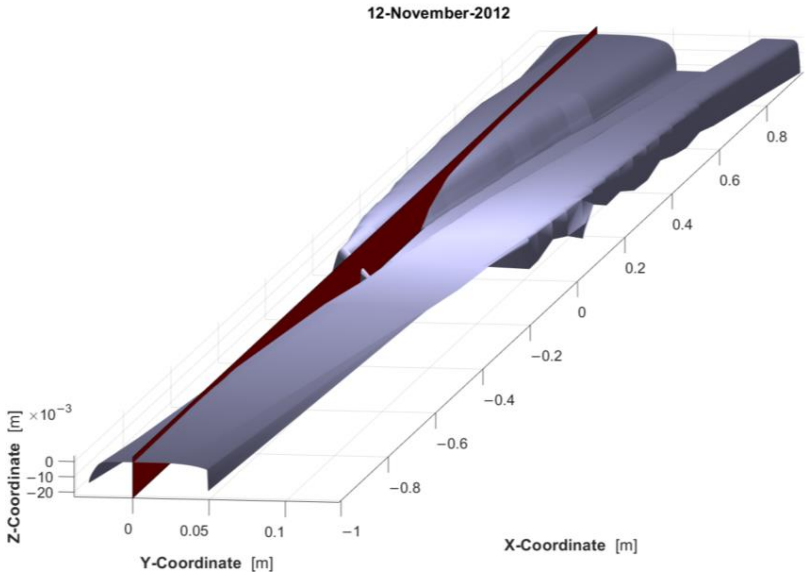

Figure 13. Mesh of reference crossing at ND5.

Figure 14a presents the profile evolution from the ND5 field data for a cross-section at the distance of 0.55 m from the crossing nose, while the corresponding profiles calculated using the SPPW method during various gross loads during service life (M01, . . . , M10) are shown in Figure 14b. To further understand and compare the SPPW predicted profiles with the field measurement data, the predicted profiles are compared to the field-measured profiles after 100 MGT, as shown in Figure 15, with high magnification. While there are slight differences, primarily due to various unaccounted variables in the actual field conditions, such as bidirectional traffic, wheel profiles, and vehicle data employed in these simulations (such as the Manchester Benchmark and a set of 14 wheel profiles) may not accurately represent the specific profiles of vehicles traversing the crossing nose, the SPPW combined with MBD simulations still predicts the profile evolution with acceptable accuracy despite the complexities of the operational environment.

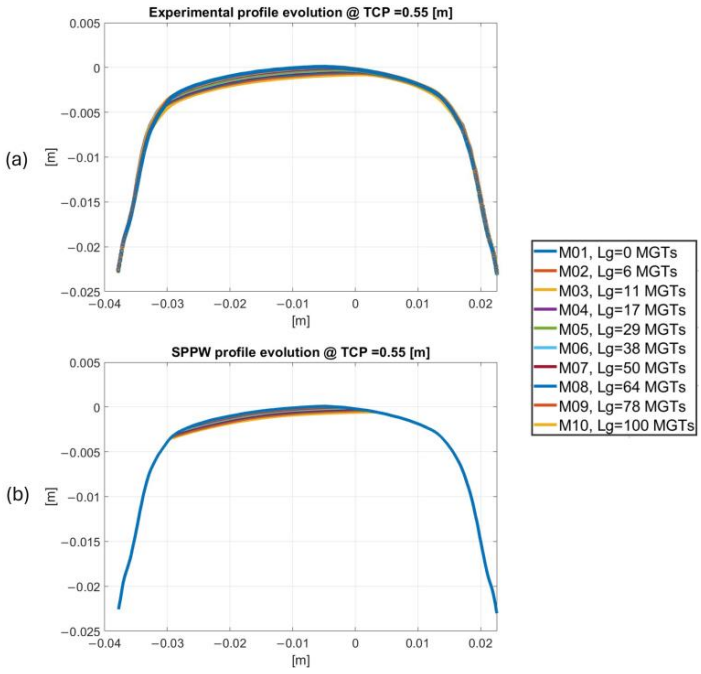

Figure 14. Crossing nose profile evolution at 0.55 m distance from TCP (**a**). Experimental profiles collected from field measurement (**b**). SPPW-predicted profiles.

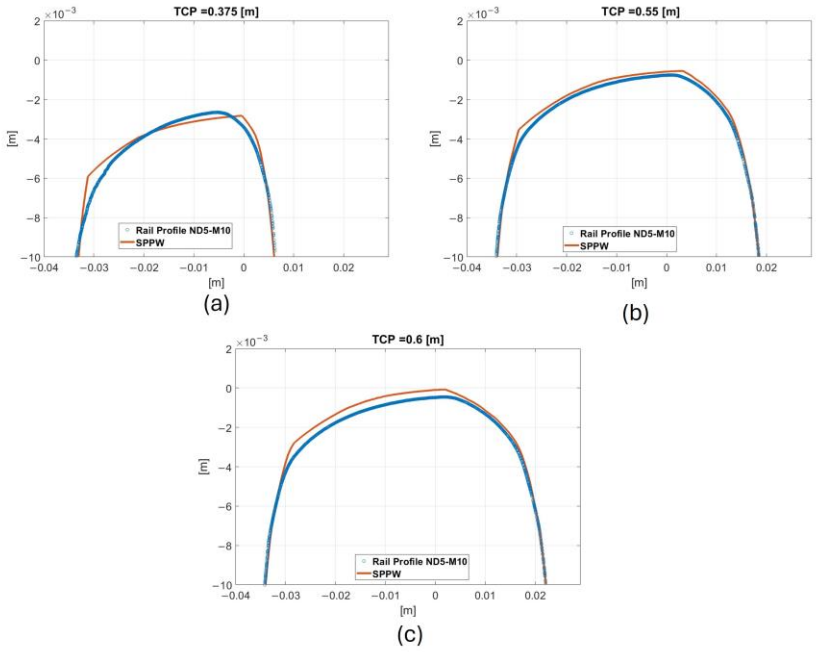

Figure 15. Crossing nose profile predicted from SPPW vs. the field measurement data after 100 MGT: (**a**). at 0.375 m distance from TCP (**b**). at 0.55 m distance from TCP (**c**). at 0.60 m distance from TCP.

6. Summary and Conclusions

In this work, the novel time-efficient semi-physical plasticity and wear model (SPPW) has been demonstrated. The main motivation for the model development was to improve the computation time of crossing rail damage simulations. Using FE-based models, typical calculation times for a WSM loop may last several weeks.

The SPPW has been developed to improve the overall efficiency of the WSM. It is based on three assumptions regarding the wear area, shape change area due to plastic deformation, and wheel profile envelope effect on the profile development due to plastic deformation and wear. Compared to the experimental results, the simulation showed a good qualitative correlation with data generated using the FE method for the R350HT steel grade and other materials. The SPPW has been shown to predict profile evolution under realistic conditions, as discussed in the case of the crossing Niklasdorf 5 (ND5) for Mn_EDH material and other materials in the case of voestalpine test rig (VTR)-modified rail.

Due to the semi-physical nature of the model, the computational time for such predictions was observed to be significantly improved compared to the analogous FE-based models using the comparable setup. Instead of several weeks, running a full loop now takes only a couple of hours, with MBD simulations proving to be the new bottleneck.

The developed model can be useful for effective and time-efficient rail surface damage prediction using the MBD simulations as a basis for the rail plastic deformation prognosis in turnouts. Moreover, as part of the whole system model framework, the developed SPPW is expected to contribute to the holistic track damage prognosis and can be used by turnout suppliers for the crossing nose design and material selection process. For example, turnout suppliers are interested in selecting the right rail material for a certain turnout depending on service conditions, including traffic load, vehicle types, shape of wheel profiles, vehicle speeds, etc. This helps to avoid the risk of unacceptable maintenance effort or too early renewal of turnout components due to wear, plastic deformation, and other damage patterns resulting in high costs. In this context, the methodology shown in Figure 1 is highly relevant. To make the method economically useful, calculation time needs to be acceptable.

Author Contributions: Conceptualization, H.D.J., K.S. (Kamil Sazgetdinov), A.M. and K.S. (Klaus Six); methodology, H.D.J., K.S. (Kamil Sazgetdinov), A.M. and K.S. (Klaus Six); software, H.D.J., K.S. (Kamil Sazgetdinov), A.M., S.S., U.O., G.M. and K.S. (Klaus Six); validation, H.D.J., K.S. (Kamil Sazgetdinov), A.M. and K.S. (Klaus Six); formal analysis, H.D.J., K.S. (Kamil Sazgetdinov), A.M., S.S., U.O., G.M. and K.S. (Klaus Six); investigation, H.D.J., K.S. (Kamil Sazgetdinov), A.M., S.S., U.O., G.M. and K.S. (Klaus Six); writing—original draft preparation, H.D.J., K.S. (Kamil Sazgetdinov), A.M. and K.S. (Klaus Six); writing—review and editing, H.D.J., K.S. (Kamil Sazgetdinov), A.M., S.S., U.O., G.M. and K.S. (Kamil Sazgetdinov); project administration, A.M.; funding acquisition, A.M. and K.S. (Klaus Six). All authors have read and agreed to the published version of the manuscript.

Funding: The study has been funded within the project Rail4Future. The project Rail4Future was funded by the program "COMET" under grant number 882504 of the Austrian Federal Ministry for Climate Action (BMK). Open Access Funding was provided by the Graz University of Technology.

Data Availability Statement: Data will be available upon request.

Acknowledgments: The publication was partly written at Virtual Vehicle Research GmbH in Graz and partially funded within the COMET K2 Competence Centers for Excellent Technologies from the Austrian Federal Ministry for Climate Action (BMK), the Austrian Federal Ministry for Labour and Economy (BMAW), the Province of Styria (Dept. 12) and the Styrian Business Promotion Agency (SFG). The Austrian Research Promotion Agency (FFG) has been authorized for the program management. The corresponding author sincerely thanks Björn Palsson for his support and assistance with the FE simulations.

Conflicts of Interest: Authors Hamed Davoodi Jooneghani, Kamil Sazgetdinov, Alexander Meierhofer, Gabor Müller and Klaus Six were employed by the company Virtual Vehicle Research GmbH. Authors Stephan Scheriau and Uwe Ossberger were employed by the company Voestalpine Rail Technology GmbH. Authors declare no conflicts of interest.

References

1. Six, K.; Sazgetdinov, K.; Kumar, N.; Müller, G.; Velic, D.; Daves, W.; Skrypnyk, R.; Pålsson, B. A whole system model framework to predict damage in turnouts. *Veh. Syst. Dyn.* **2021**, *61*, 871–891. [CrossRef]
2. Kumar, N.; Kossmann, C.; Scheriau, S.; Six, K. An efficient physical-based method for predicting the long-term evolution of vertical railway track geometries. *Proc. Inst. Mech. Eng. Part F J. Rail Rapid Transit* **2022**, *236*, 447–465. [CrossRef]
3. Ohno, N.; Wang, J.-D. Kinematic hardening rules with critical state of dynamic recovery, part I: Formulation and basic features for ratchetting behavior. *Int. J. Plast.* **1993**, *9*, 375–390. [CrossRef]
4. Archard, J.F. Contact and Rubbing of Flat Surfaces. *J. Appl. Phys.* **1953**, *24*, 981–988. [CrossRef]
5. Skrypnyk, R.; Nielsen, J.C.O.; Ekh, M.; Pålsson, B.A. Metamodelling of wheel–rail normal contact in railway crossings with elasto-plastic material behaviour. *Eng. Comput.* **2018**, *35*, 139–155. [CrossRef]
6. Meyer, K.A.; Skrypnyk, R.; Pletz, M. Efficient 3d finite element modeling of cyclic elasto-plastic rolling contact. *Tribol. Int.* **2021**, *161*, 107053. [CrossRef]
7. Spangenberg, U.; Fröhling, R.D.; Els, P.S. Long-term wear and rolling contact fatigue behaviour of a conformal wheel profile designed for large radius curves. *Veh. Syst. Dyn.* **2019**, *57*, 44–63. [CrossRef]
8. Sazgetdinov, K.; Meierhofer, A.; Scheriau, S.; Ossberger, U.; Palsson, B.; Six, K. A semi-physical model to predict plasticity in railway turnout crossings. In Proceedings of the CM 2022—12th International Conference on Contact Mechanics and Wear of Rail/Wheel Systems, Conference Proceedings. Melbourne, VIC, Australia, 4–7 September 2022; pp. 749–754.
9. Johansson, A.; Pålsson, B.; Ekh, M.; Nielsen, J.C.; Ander, M.K.; Brouzoulis, J.; Kassa, E. Simulation of wheel–rail contact and damage in switches & crossings. *Wear* **2011**, *271*, 472–481. [CrossRef]
10. Niklitsch, D.; Nielsen, J.; Ekh, M.; Johansson, A.; Pålsson, B.; Zoll, A. Simulation of wheel–rail contact and subsequent material degradation in switches & crossings. In Proceedings of the 21st International Symposium on Dynamics of Vehicles on Roads and Tracks, Stockholm, Sweden, 17–21 August 2009; p. 14.
11. Xin, L.; Markine, V.; Shevtsov, I. Numerical procedure for fatigue life prediction for railway turnout crossings using explicit finite element approach. *Wear* **2016**, *366–367*, 167–179. [CrossRef]
12. Bezin, Y.; Pålsson, B.; Kik, W.; Schreiber, P.; Clarke, J.; Beuter, V.; Sebes, M.; Persson, I.; Magalhaes, H.; Wang, P.; et al. Multibody simulation benchmark for dynamic vehicle–track interaction in switches and crossings: Results and method statements. *Veh. Syst. Dyn.* **2021**, *61*, 660–697. [CrossRef]

13. Bezin, Y.; Pålsson, B.A. Multibody simulation benchmark for dynamic vehicle-track interaction in switches and crossings: Modelling description and simulation tasks. *Veh. Syst. Dyn.* **2021**, *61*, 644–659. [CrossRef]
14. Pålsson, B.A. Optimisation of railway crossing geometry considering a representative set of wheel profiles. *Veh. Syst. Dyn.* **2015**, *53*, 274–301. [CrossRef]
15. Skrypnyk, R.; Pålsson, B.A.; Nielsen, J.C.O.; Ekh, M. On the influence of crossing angle on long-term rail damage evolution in railway crossings. *Int. J. Rail Transp.* **2021**, *9*, 503–519. [CrossRef]
16. Gschwandl, T.J.; Weniger, T.M.; Antretter, T.; Künstner, D.; Scheriau, S.; Daves, W. Experimental and Numerical Visualisation of Subsurface Rail Deformation in a Full-Scale Wheel–Rail Test Rig. *Metals* **2023**, *13*, 1089. [CrossRef]
17. Oldknow, K.; Stock, R.; Vollebregt, E. Effects of rail hardness on transverse profile evolution and computed contact conditions in a full-scale wheel-rail test rig evaluation. *Wear* **2024**, *560–561*, 4–7. [CrossRef]
18. Fuchs, J.; Müller, G.; Sazgetdinov, K.; Wipfler, E.; Nerlich, I. A methodology for alignment of measured rail profiles in turnouts as a basis for reliable vehicle/track interaction simulations. *Veh. Syst. Dyn.* **2021**, *61*, 821–837. [CrossRef]